

# Optimized stray-field-induced enhancement of the electron spin precession by buried Fe gates

L. Meier\*, G. Salis and N. Moll

*IBM Research, Zurich Research Laboratory, Säumerstrasse 4, 8803 Rüschlikon, Switzerland*

C. Ellenberger, I. Shorubalko, U. Wahlen and K. Ensslin

*Solid State Physics Laboratory, ETH Zurich, 8093 Zurich, Switzerland*

E. Gini

*FIRST Center for Micro- and Nanosciences, ETH Zurich, 8093 Zurich, Switzerland*

(Dated: 27. August 2007)

The magnetic stray field from Fe gates is used to modify the spin precession frequency of InGaAs/GaAs quantum-well electrons in an external magnetic field. By using an etching process to position the gates directly in the plane of the quantum well, the stray-field influence on the spin precession increases significantly compared with results from previous studies with top-gated structures. In line with numerical simulations, the stray-field-induced precession frequency increases as the gap between the ferromagnetic gates is reduced. The inhomogeneous stray field leads to additional spin dephasing.

The magnetic stray field from a confined ferromagnetic structure is spatially strongly inhomogeneous. It decays on the length scale of the magnetic object. Magnetic stray fields have many applications ranging from data storage to future technologies such as quantum computation [1] or spintronics [2]. The spatial field distribution from ferromagnetic structures has been characterized by magnetic-force microscopes [3, 4] or scanning Hall probes [5]. The influence of stray fields on nearby semiconductor spin-states has been investigated by photoluminescence [6, 7], spin-flip light scattering [8], cathodoluminescence [9] and time-resolved Faraday rotation [10, 11] in semiconductor quantum wells (QWs).

In previous experiments [10], we reported that the electron spin precession frequency  $\nu$  of electrons in a QW below an array of Fe stripes increases proportionally to the component of the Fe magnetization perpendicular to the stripes and in-plane of the QW. This enhancement of  $\nu$  was less than expected from a homogeneous average over the stray field in the gap between two Fe stripes, and depended non-monotonically on the geometry of the stripes. These discrepancies were attributed [10, 11] to near-field optical effects and enhanced transmission close to the metallic stripes, leading to the probing of electron spins not only in the gap between two Fe stripes, but also below the stripes, where the stray field points into the opposite direction of the external magnetic field [Fig. 1(b), situation ‘top’].

In this letter, we show that the stray-field-induced enhancement of  $\nu$  can be considerably increased if the Fe stripes are brought into the plane of the QW by an etching process, thereby eliminating the contributions of regions where the stray field points against the exter-

nal magnetic field. This stray-field influence on  $\nu$  is in good agreement with micromagnetic stray-field simulations. We find a monotonous increase of this enhancement when decreasing the width of the stripes and the gap between two stripes, in line with theoretical expectations. The spin decay-rate is increased by an amount that is proportional to the stray-field-induced increase in precession frequency, providing evidence of the occurrence of inhomogeneous broadening.

We use time-resolved Faraday rotation (TRFR) [12] in the Voigt geometry to measure the spin-precession frequency of optically excited electron spins in a GaAs/InGaAs QW structure. A first, circularly-polarized pump pulse (pulse duration 3 ps, repetition rate 80 MHz at an average power of 400  $\mu$ W, focus diameter 15  $\mu$ m) excites spin-polarized electrons into the conduction band. The spin polarization initially points perpendicularly to the QW plane, along the  $z$ -direction. After a delay  $\Delta t$ , the spin polarization  $S_z$  along  $z$  is monitored by measuring the angle  $\theta_F \propto S_z$ , by which the polarization plane of a second, linearly polarized laser pulse (pulse power 60  $\mu$ W) is rotated. The signal obtained by sweeping  $\Delta t$  between 0 and 2 ns fits well to  $\theta_F(\Delta t) = \theta_0 \cos(2\pi\nu\Delta t) \exp(-t/T_2^*)$ , where the exponential accounts for the finite spin lifetime  $T_2^*$  and  $\nu = g\mu_B B_{\text{tot}}/h$  is proportional to the total magnetic field  $B_{\text{tot}}$  in the plane of the QW, with  $g$  the electron  $g$ -factor,  $\mu_B$  the Bohr magneton and  $h$  Planck’s constant. By measuring  $\nu$ , we can determine the total local magnetic field  $B_{\text{tot}} = B_{\text{ext}} + \langle B_s \rangle$  within the laser focus spot with a precision of  $\approx 1$  MHz (corresponding to  $\approx 0.1$  mT). Here,  $B_{\text{ext}}$  is an externally applied magnetic field in the plane of the QW and perpendicular to the stripe’s long axis. The spatially inhomogeneous stray field is averaged over the laser spot and contributes with  $\langle B_s \rangle$  to the total field. To minimize additional effective magnetic fields from nuclear polarization, we switch between left- and right-hand

---

\*Also at: Solid State Physics Laboratory, ETH Zurich, 8093 Zurich, Switzerland

circularly-polarized pump light at 50 kHz and measure at a temperature of  $T = 40$  K [10].

Our sample is a 40-nm-wide GaAs/InGaAs QW (8.8% In), with a bulk Si-doping in the QW aimed at  $5 \times 10^{16} \text{ cm}^{-3}$ . The QW is capped by 20 nm of GaAs,  $\delta$ -doped with Si to compensate for surface states. In this case, the spin measurements are not limited by the finite recombination time ( $\approx 300$  ps) of optically excited electrons. Using electron-beam lithography, arrays of stripes with a width  $w$  and separated by a distance  $w$ ,  $w \approx 1, 2$  and  $3 \mu\text{m}$ , are patterned into a double-layered PMMA resist that is approximately 300 nm high. The resulting gratings are 100 by 100  $\mu\text{m}$  in size. The sample is then etched with a reactive-ion etching (RIE) process with 7 standard cubic centimeters per minute (sccm)  $\text{CH}_4$ , 50 sccm  $\text{H}_2$ , 5 sccm Ar, 3 sccm  $\text{Cl}_2$  and an r.f. power of 135 W (frequency 13.56 MHz) at  $T = 95^\circ\text{C}$  during twice 25 s, interrupted by 5 min of  $\text{N}_2$  flushing. The resulting 100-nm-deep trenches [see Fig. 1(d)] are filled by the evaporation of 10 nm Ti, 80 nm Fe and 10 nm Al. After a lift-off process, the stripes are buried in the GaAs, centered about the QW in  $z$ -direction, as schematically shown in the upper inset of Fig. 1(a).

A TRFR sweep with the laser focused on a grating ( $w \approx 1 \mu\text{m}$ ) with  $B_{\text{ext}} = 1.05$  T is shown by the thick line in Fig. 1(a). Compared with a sample in which the Fe has been replaced by Au (thin line),  $\nu$  is enhanced by  $\Delta\nu = \nu_{\text{Fe}} - \nu_{\text{Au}} = 1.12$  GHz, which is attributed to the magnetic stray field. Away from the magnetic stripes, we determine  $g = 0.520$  and thus find  $\langle B_s \rangle = h\Delta\nu/g\mu_B = 154$  mT. This is about 8 times larger than previous results on top-gated structures with the same stripe geometry [10]. The spatially inhomogeneous  $B_s$  leads to a distribution of precession frequencies in the spin ensemble. The resulting dephasing rate  $\tau^{-1}$  can be approximated by  $\tau 2\pi\delta\nu = 1$ , where  $\delta\nu$  is an effective spread of precession frequencies. It can be extracted from the experiment by using  $\tau^{-1} = (T_{2,\text{Fe}}^*)^{-1} - (T_{2,\text{Au}}^*)^{-1}$ , and yields  $\delta\nu \approx 334$  MHz, about three times smaller than  $\Delta\nu$ .

A micromagnetic simulation of the magnetic stray field obtained with OOMMF [13] is shown in Fig. 1(b). In the top panel, the geometrical orientation of the stray field between two magnetized Fe stripes is shown for the structure with QW between the buried stripes, and for the structure with the stripes evaporated on top of the sample surface [see inset of Fig. 1(a)]. The  $x$ -component of the stray field, which our measurement geometry is mainly sensitive to, is shown in the lower panel of Fig. 1(b). The peak stray-field in the samples with buried gates is approximately 10 times larger than in the top-gated structures. A spatially homogeneous average for the buried structure over  $B_s^x(x)$  between the stripes [ $0.5 \mu\text{m} < x \leq 1.5 \mu\text{m}$  in Fig. 1(b)] yields  $\langle B_s \rangle = 107$  mT for  $w = 1 \mu\text{m}$  and  $B_{\text{ext}} = 1$  T.

Figure 2(a) shows the measured  $\Delta\nu$  as a function of  $B_{\text{ext}}$ . At  $B_{\text{ext}} = 0$ , the Fe stripes are magnetized along their long (easy) axis in the  $y$ -direction, and no stray field in the  $x$ -direction is expected. As  $B_{\text{ext}}$  increases,

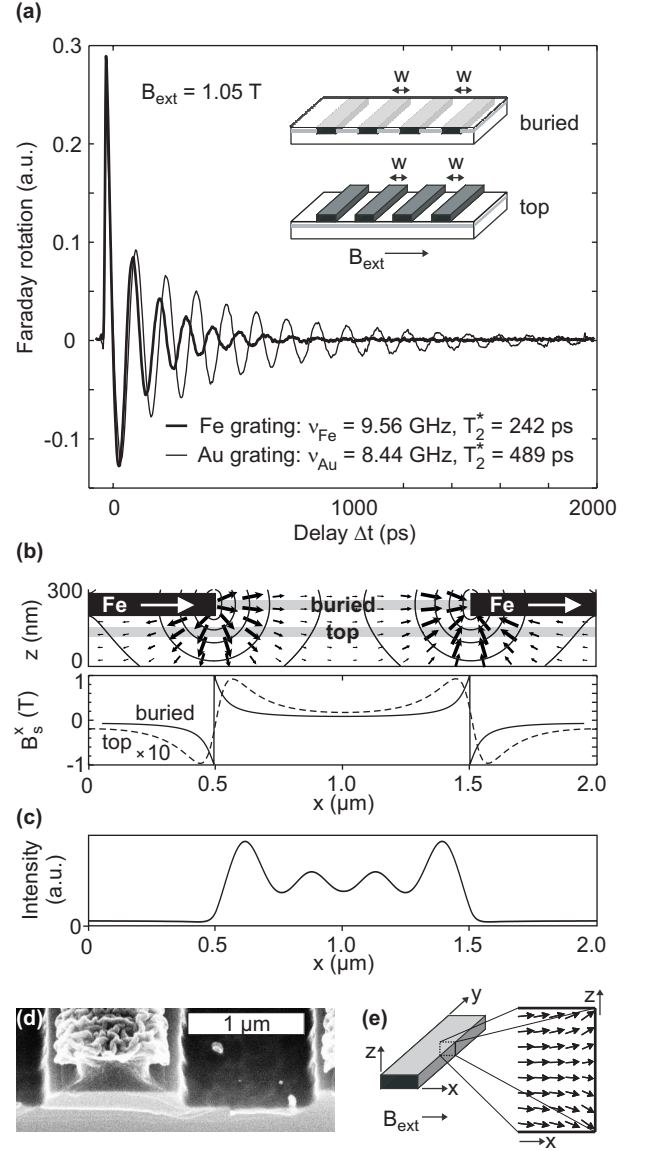


FIG. 1: (a) TRFR oscillations on a Fe (thick line) and a Au (thin line) grating ( $w \approx 1 \mu\text{m}$ ). Inset: sample structure with buried and top-gated Fe stripes. (b) Top: Numerical simulation of the magnetic stray field  $B_s$ . Bottom: Numerical simulation of the  $x$ -component of  $B_s$  for buried and top-gated sample structures. (c) Simulated illumination intensity of the QW between two Fe stripes for the buried structure. (d) Etched GaAs sample with double-layer PMMA mask. (e) Simulation of the Fe stripe magnetization ( $w = 3 \mu\text{m}$ ), in an external magnetic field  $B_{\text{ext}} = 500$  mT. Cut through the  $x/z$  plane.

the magnetization turns towards  $x$ . For smaller stripe widths  $w$ , larger  $B_{\text{ext}}$  are needed to magnetize the Fe along  $x$  because of shape anisotropy. This is verified by MOKE measurements [10], and reflected in the shape of  $\Delta\nu$  vs.  $B_{\text{ext}}$ . This effect is also visible in the simulation in Fig. 2(c). Here, the magnetization  $\mathbf{m}$  of the Fe stripes has been calculated as a function of  $B_{\text{ext}}$ , and from  $\mathbf{m}$ , we obtain the homogeneously averaged stray field. After

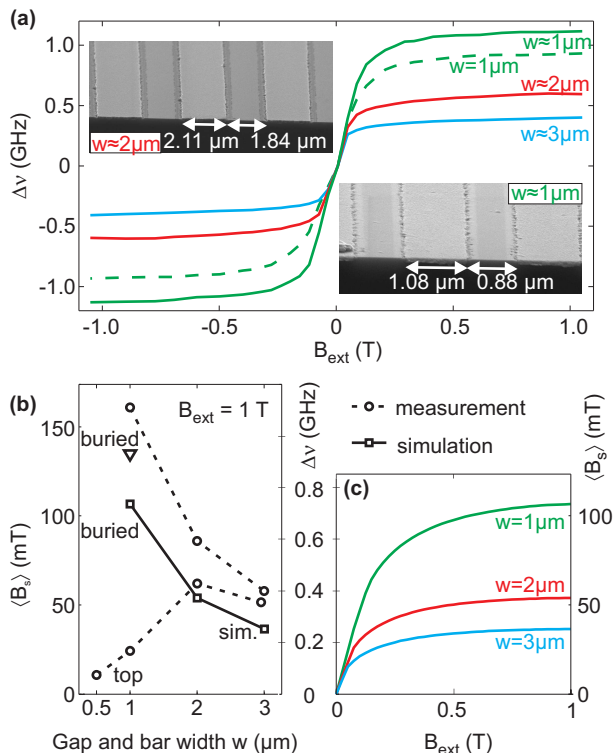


FIG. 2: (Color online) (a) Enhancement of the electron spin precession frequency  $\Delta\nu$  as a function of  $B_{\text{ext}}$  for different gap and stripe widths  $w$  (solid lines). Inset: Because of the etching process, the stripes are slightly too wide and the gaps too narrow. The dashed line shows  $\Delta\nu$  for a sample with equal gap and stripe width  $w = 1 \mu\text{m}$ . (b)  $\langle B_s \rangle$  and  $\Delta\nu$  for different  $w$  at  $B_{\text{ext}} = 1 \text{ T}$  as measured (dashed lines) for buried and top-gated and as simulated (solid line) for buried structures. Triangle: Measured  $\langle B_s \rangle$  for the compensated  $w = 1 \mu\text{m}$  sample. (c) Simulated  $\langle B_s \rangle$  and  $\Delta\nu$  as a function of  $B_{\text{ext}}$  for different  $w$  (buried structures).

a roughly linear increase of  $\langle B_s \rangle$  due to the rotation of  $\mathbf{m}$  from along  $y$  into the  $x/z$  plane,  $\langle B_s \rangle$  slowly increases. This increase is due to  $\mathbf{m}$ , which, in the corners of the  $x/z$  plane [see Fig. 1(e)], has components along  $z$  that decrease as  $B_{\text{ext}}$  is increased. If all magnetic moments in the Fe stripes point along the  $x$ -direction, i.e.  $\mathbf{m} = m\hat{x}$ , the value of  $\langle B_s \rangle$  saturates.

The measured and calculated values of  $\Delta\nu$  and  $\langle B_s \rangle$  at  $B_{\text{ext}} = 1 \text{ T}$  are plotted in Fig. 2(b) for varying gap and stripe widths  $w$ . In the structure with buried stripes, the stray-field-induced enhancement of  $\nu$  decreases with  $w$  in both measurement and simulation. Because the magnetic stray field between two Fe gates stems from the finite divergence of the magnetization at its boundary, here mainly in the  $y/z$  plane, the gate's extension in the  $x$ -direction has only a minor influence on  $B_s$ . The average  $\langle B_s \rangle$  is predominated by the high values of  $B_s(x)$  for  $x$  close to a stripe edge, which is independent of the stripe width. With increasing  $w$ ,  $\langle B_s \rangle$  decreases roughly as  $1/w$  because more and more of the gap region sees a negligible

stray-field strength. In our previous work with top-gated structures [10], we observed a non-monotonous dependence of  $\Delta\nu$  on  $w$  [see the dashed line 'top' in Fig. 2(b)] owing to the probing of negative stray fields in regions below the stripe, which were illuminated because of effects due to enhanced optical transmission.

While the qualitative behavior of the buried gates is similar in experiment and simulation, the absolute value of  $\langle B_s \rangle$  is about 50% higher in the experiment than in the simulation. This is partly due to the fact that the RIE process etches the mask also slightly laterally, leading to stripes that are  $\approx 100 \text{ nm}$  wider than the original mask, at the cost of narrower gaps [see the SEM images in the insets of Fig. 2(a)]. By using a compensated mask geometry with narrower stripes, the resulting  $\langle B_s \rangle$  decreases in the experiment, as shown by the dashed line in Fig. 2(a) and the triangle in Fig. 2(b) for a  $w = 1 \mu\text{m}$  grating.

Still,  $\langle B_s \rangle$  exceeds the numerically expected values by about 25%. This may be explained by a non-homogeneous averaging of the stray field in the gap. Numerical simulations of the light intensity distribution [finite-difference time-domain, Fig. 1(c)] reveal an enhanced intensity close to a stripe edge. Therefore, these regions with higher-than-average stray fields contribute more to the spatial average and may lead to an elevated  $\langle B_s \rangle$ . However, the simulation predicts a sharp drop of the light intensity at the metal edge as well, which leads to an underrepresentation of the peak stray-field values (compared with a homogeneous average) and neutralizes the former effect. We note that also the sensitivity of TRFR angle on spin polarization may be spatially modulated owing to near-field optical effects, leading to additional weighting of the stray-field average. A detailed description of this effect would exceed the scope of this paper.

Also the spin lifetimes exhibit a strong dependence on  $w$ . As described previously, the additional decoherence rate  $\tau^{-1}$  and thereby the stray-field magnitude can be estimated from  $T_2^*$ . We find  $\delta\nu = 334, 191$  and  $72 \text{ MHz}$  for the  $w \approx 1, 2$  and  $3 \mu\text{m}$  gratings, respectively. Although the total spread of the stray field is independent of  $w$ , the effective spread  $\delta\nu$  is diluted by increasing  $w$  (because more volume with negligible stray field is added), leading to a decrease of  $\delta\nu$ , in line with  $\Delta\nu$  determined from the spin-precession frequency.

In conclusion, we have measured the effect of magnetized Fe gates on the electron spin-precession frequency  $\nu$ . By etching the gates down to the quantum well, the numerically expected average stray field  $\langle B_s \rangle$  between two stripes is increased by a factor of  $\approx 3$ , compared with the situation with top-gated Fe electrodes. In the experiment,  $\nu$  is increased by up to one order of magnitude for samples with buried gates, because here near-field optical effects do not lead to the probing of regions with stray fields pointing along the negative  $x$ -direction, as it is the case for top-gated structures.

- 
- [1] D. Loss and D. P. DiVincenzo, Phys. Rev. A **57**, 120 (1998).
- [2] S. Datta and B. Das, Appl. Phys. Lett. **56**, 665 (1990).
- [3] Y. Martin and H. K. Wickramasinghe, Appl. Phys. Lett. **50**, 1455 (1987).
- [4] A. Winkler, T. Muhl, S. Menzel, R. Kozhuharova-Koseva, S. Hampel, A. Leonhardt, and B. Buchner, J. Appl. Phys. **99**, 104905 (2006).
- [5] A. M. Chang, H. D. Hallen, L. Harriott, H. F. Hess, H. L. Kao, J. Kwo, R. E. Miller, R. Wolfe, J. van der Ziel, and T. Y. Chang, Appl. Phys. Lett. **61**, 1974 (1992).
- [6] H. Schömig, A. Forchel, S. Halm, G. Bacher, J. Puls, and F. Henneberger, Appl. Phys. Lett. **84**, 2826 (2004).
- [7] M. Sakuma, K. Hykomi, I. Souma, A. Murayama, and Y. Oka, Appl. Phys. Lett. **85**, 6203 (2004).
- [8] M. Sakuma, K. Hyomi, I. Souma, A. Murayama, and Y. Oka, J. Appl. Phys. **94**, 6423 (2003).
- [9] J. Kossut, I. Yamakawa, A. Nakamura, G. Cywiński, K. Fronc, M. Czczott, J. Wróbel, F. Kyrychenko, T. Wojtowicz, and S. Takeyama, Appl. Phys. Lett. **79**, 1789 (2001).
- [10] L. Meier, G. Salis, C. Ellenberger, K. Ensslin, and E. Gini, Appl. Phys. Lett. **88**, 172501 (2006).
- [11] L. Meier, G. Salis, C. Ellenberger, E. Gini, and K. Ensslin, Phys. Rev. B **74**, 245318 (2006).
- [12] S. A. Crooker, D. D. Awschalom, and N. Samarth, IEEE J. Sel. Top. Quantum Electron. **1**, 1082 (1995).
- [13] <http://math.nist.gov/oommf/>.